Causes and Consequences of Variations in Faulting Style at the Mid-Atlantic Ridge

PETER R. SHAW AND JIAN LIN

Woods Hole Oceanographic Institution, Woods Hole, Massachusetts

Both volcanism and faulting contribute to the rugged topography that is created at the Mid-Atlantic Ridge (MAR) and preserved off-axis in Atlantic abyssal hill terrain. Distinguishing volcanic from fault-generated topography is essential to understanding the variations in these processes and how these variations are affected by the three-dimensional pattern of mantle upwelling, ridge segmentation, and offsets. Here we describe a new quantitative method for identifying fault-generated topography in swath bathymetry data by measuring topographic curvature. The curvature method can distinguish large normal faults from volcanic features, whereas slope methods cannot because both faults and volcanic constructs can produce steep slopes. The combination of curvature and slope information allows inward and outward facing fault faces to be mapped. We apply the method to Sea Beam data collected along the MAR between 28° and 29°30'N. The fault styles mapped in this way are strongly correlated with their location within the ridge segmentation framework: long, linear, small-throw faults occur toward segment centers, while shorter, larger-throw, curved faults occur toward ends; these variations reflect those of active faults within the axial valley. We investigate two different physical mechanisms that could affect fault interactions and thus underlie variations in abyssal hill topography at the MAR. In the first model only one fault is active at a time on each side of the rift valley. Each fault grows while migrating away from the volcanic center due to dike injection; extension across the fault causes a flexural rotation of nearby inactive faults. The amount of stress necessary to displace the fault increases as the fault grows. When reaching a critical size the fault stops growing as fault activity jumps inward as a new fault starts its growth near the rift valley. This model yields a realistic terracelike morphology from the rift valley floor into the rift mountains; the relief is caused by the net rotation accumulated in the lithosphere from the active faults (e.g., 10° reached 20 km from the active fault). Fault spacing is controlled by lithospheric thickness, fault angle, and the ratio of amagmatic to magmatic extension. We hypothesize that this mechanism may be dominant toward ridge segment offsets. An alternative model considers multiple active faults; each fault relieves stresses as it grows and inhibits the growth of nearby faults, causing a characteristic fault spacing. Such fault interactions would occur in a region of necking instability involving deformation over an extended area. This mode of extension would drive a feedback mechanism that would act to regulate the size of nearby faults. We hypothesize that this mechanism may be active in the relatively weak regions of strong mantle upwelling near segment midpoints, causing the homogeneous abyssal hill fabric in these regions.

1. INTRODUCTION

Detailed views of the Mid-Atlantic Ridge (MAR) between 24° and 31°N from recently collected Sea Beam data [*Sempéré et al.*, 1990, 1993; *Purdy et al.*, 1990] reveal a fundamental segmentation of the ridge with length scales 10–100 km. The segmentation is expressed primarily through offsets of the axial valley and the deepening and widening of the valley toward each segment end. The mantle Bouguer anomaly (MBA) in this region [*Lin et al.*, 1990] defines a series of bulls-eye-shaped negative anomalies, interpreted as some combination of thick crust and light mantle, which could occur over a mantle upwelling center. The morphology and overall depth of the rift valley and the nature of the rift valley bounding faults are closely related to the MBA; the valley is narrowest and the bounding faults most linear toward ridge segment centers, particularly over those centers associated with strong MBA lows [*Sempéré et al.*, 1990, 1993].

Within the MAR median valley, volcanism is one of the most significant processes active in producing the topography. Crust is formed through centers of constructional volcanism at the axial volcanic ridge (AVR), a linear feature

composed of numerous small volcanic edifices [e.g., *Needham and Francheteau*, 1974; *Macdonald et al.*, 1975; *Ballard and van Andel*, 1977; *Luyendyk and Macdonald*, 1977; *Smith and Cann*, 1990, 1992]. The relief of the volcanic constructs often matches the relief of the rugged topography found in the abyssal mountains and abyssal hills [*Macdonald and Atwater*, 1978; *Pockalny et al.*, 1988; *Kappel and Ryan*, 1986; 1991; *Kong et al.*, 1988; *Smith and Cann*, 1990, 1992]. Starting at distances of 1–4 km from the AVR, the growth of large normal faults plays an important role in the development of topography seen off-axis.

The role of faulting in the formation of Atlantic abyssal hills has been the subject of a number of investigations [*Rona et al.*, 1974; *Whitmarsh and Laughton*, 1976; *Macdonald and Luyendyk*, 1977; *Kappel and Ryan*, 1991; *Kong et al.*, 1988; *Pockalny et al.*, 1988]. At intermediate spreading rates the locations where new normal faults grow can be closely related to volcanism: at the Juan de Fuca ridge the axial volcanic ridge is observed to be split by faults within the median valley, forming the basis of abyssal hill morphology [*Kappel and Ryan*, 1986]. Along the slower spreading Mid-Atlantic Ridge, interactions of faults and volcanism are observed in the form of volcanic constructs at the edges of the normal fault foot walls [*Macdonald et al.*, 1975; *Macdonald and Luyendyk*, 1977; *Kappel and Ryan*, 1991]. The edges of the axial volcanic ridge may thus become preferred sites for the growth of new faults, although alternatively, it is possi-

ble that this association occurs by volcanic extrusion along fault planes.

The process of faulting is considered to be governed by the overall state of stress in the lithosphere as well as the overall lithospheric thickness and strength in a number of models [*Vening Meinesz*, 1950; *Rundle*, 1982; *King et al.*, 1988; *Stein et al.*, 1988; *Buck*, 1988; *Weissel and Karner* 1989; *Forsyth*, 1992]. The conceptual model of *Lin et al.* [1990] predicts stronger mantle upwelling, shallower isotherms, and thus weaker lithosphere toward MAR segment centers associated with strong MBA lows, providing a basis for along-axis changes in the faulting process. Studies of earthquake location in this part of the Atlantic [*Lin and Bergman*, 1990] show that large earthquakes cluster toward segment ends, independently suggesting a general increase in brittle strength toward the end of ridge segments.

In this paper we analyze Sea Beam bathymetry between 28°N and 29°30'N from a survey of a larger area of the MAR [*Purdy et al.*, 1990]. We describe in detail a method designed to distinguish faults from other rugged morphology through the measurement of topographic curvature in multibeam bathymetric data; the method has been applied by *Shaw* [1992]. We study the variability of the faulting process through the identification of faults at different scales in order to study along-axis changes in lithospheric strength. Significant differences are observed in the spacing and throw of faults between segment centers and segment ends. We then propose two alternative models to explain the variations of observed fault parameters in terms of changes in lithospheric properties such as brittle thickness.

2. METHODS

2.1. Slope Analysis

Scarps originating from large-throw faults can have dips of approximately 50°–60° [*Macdonald and Luyendyk*, 1977]; using topographic slopes would thus appear to be one po-

tential criterion for identifying the faults in the Sea Beam bathymetric data, although the finite resolution of the Sea Beam system smooths the measured bathymetry, reducing the apparent slopes. Slopes are also useful for quantifying the overall character of seafloor [*Shaw and Smith*, 1987, 1990; *Smith and Shaw*, 1989]. Figure 1a shows a map of topographic slopes for a portion of Sea Beam bathymetry that includes the median valley near 29°N (this same sample is further analyzed in Plate 1). The bathymetric data analyzed here has been gridded at a spacing of 150 m. Lineations that we infer to be related to fault scarps are visible as a series of roughly linear loci of large (> 20–25°) slope. However, the map also highlights other features such as volcanic constructions and mass-wasting features; these features can also have large slopes [e.g., *Tucholke*, 1992]. Thus slope angle alone cannot uniquely identify faults.

2.2. Curvature Analysis

Formulation. We measure topographic curvature by approximating topography falling within a small circular aperture with the quadratic surface z defined over coordinates (x, y):

$$z(x, y) = a_{11}x^2 + a_{22}y^2 + 2a_{12}xy + b_1 x + b_2 y + c$$
$$= v^T A v + b^T v + c \qquad (1)$$

where

$$v = \begin{bmatrix} x \\ y \end{bmatrix}, \quad A = \begin{bmatrix} a_{11} & a_{12} \\ a_{12} & a_{22} \end{bmatrix}, \quad b = \begin{bmatrix} b_1 \\ b_2 \end{bmatrix}. \qquad (2)$$

The radius of the aperture is an additional parameter that does not explicitly enter the formulation (1) and (2). The six free parameters $\{a_{11}, a_{22}, a_{12}, b_1, b_2, c\}$ are found in a linear least squares sense [e.g., *Menke*, 1984]. The quantities of interest are the two principal curvatures of the surface, $\{k_1, k_2\}$, which are the eigenvalues of A [e.g., *Bronshtein and Semendyayev*, 1985]; here we order these $k_1 \leq k_2$. Prin-
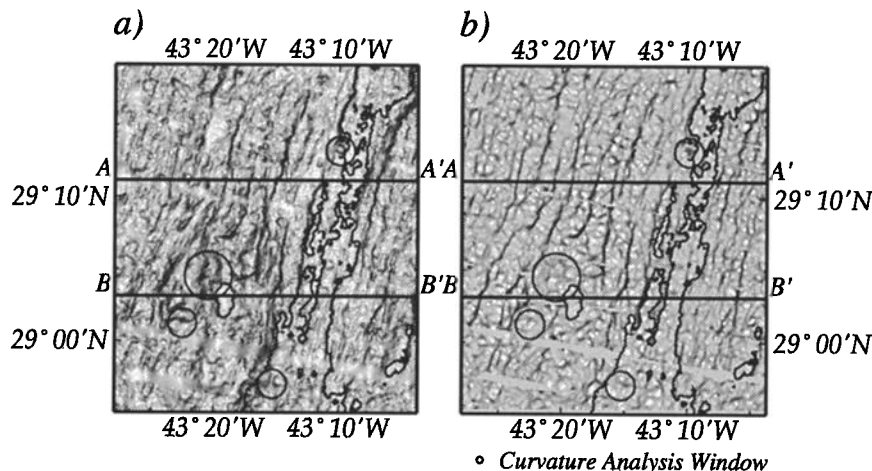

Fig. 1. Comparison of feature flagging by slope magnitude and by curvature magnitude. (*a*) Map of topographic slope magnitude for sample of MAR topography; 3200-m contour is drawn to indicate general outline of the rift valley. Map region and profiles A-A' B-B' are the same as Plate 1. The rift mountains, which evolve into abyssal hills, appear as highlighted linear features outside the valley. Constructs within the median valley such as the AVR and circular features inferred to be seamounts on the basis of their distinctive forms often yield slopes comparable to those associated with the rift mountains. Circles are drawn around several volcanic features with significant slopes. (*b*) Map of topographic curvature (k_1) values, calculated with the 0.45-km-radius window (window size is indicated below figure). Footwall corners, forming the rift mountain lineations, appear in both maps, whereas the circled features have steep slopes but not sharp curvature. The image of topographic curvature values thus emphasizes the sharp features and serves to distinguish fault-derived topography from that produced by volcanics and mass wasting.

cipal curvatures are computed for each position of the circular window as it is scanned across the data grid, producing values of k_1 and k_2 at each point of the same spatial grid.

Figure 2 shows several samples of topography together with their representation by quadratic surfaces. We use the most negative principal curvature, k_1, of the surface z to quantify the topography. If $k_1 < 0$, the feature is concave-down and is a peak, ridge, or saddle, depending on sign of k_2. The parameter k_1 alone, such as shown in Figure 1, is generally sufficient to delineate well-defined lineaments that we interpret as an expression of fault scarps.

Varying analysis window size. The differences in the throw and spacing of fault scarps at the Mid-Atlantic Ridge can be pronounced. We seek to quantify this first-order variability by varying the aperture of the analysis window. If the data window in curvature fitting is large enough to encompass several ridges, the single quadratic surface will be relatively flat and not representative of any of the individual ridges (Figure 2b). The surface will have greater success modeling a single ridge isolated within the window, which happens when the window diameter is comparable or

smaller than the ridge spacing, as in Figures 2a and 2c. This property provides a means of measuring the dimensions of individual scarps when the curvature calculation is repeated at a range of aperture sizes. Varying the size of the window therefore allows bathymetry to be mapped at a series of scales to determine the spatial distribution of features.

Comparison with slopes. A map of the principal curvature values k_1 computed at the 0.45 km scale is shown for the sample region in Figure 1b. In the curvature map, scarps appear as the elongate dark loci and are more distinct than in the slope map. The scarps thus seem to have a relatively unique curvature signature that allows them to be distinguished from volcanic constructs. Several regions (circled) associated with steep slopes are lacking in significant curvature, indicating that they are probably not associated with faults. Significantly, the median valley is nearly devoid of scarps. This example sheds some light on the question of whether the abyssal hill fabric in this area originates from cast-off axial volcanic ridges [e.g., *Kappel and Ryan*, 1991; *Pockalny et al.*, 1988] or from the growth of normal faults [e.g., *Laughton and Rusby*, 1975; *Whitmarsh and Laughton*,
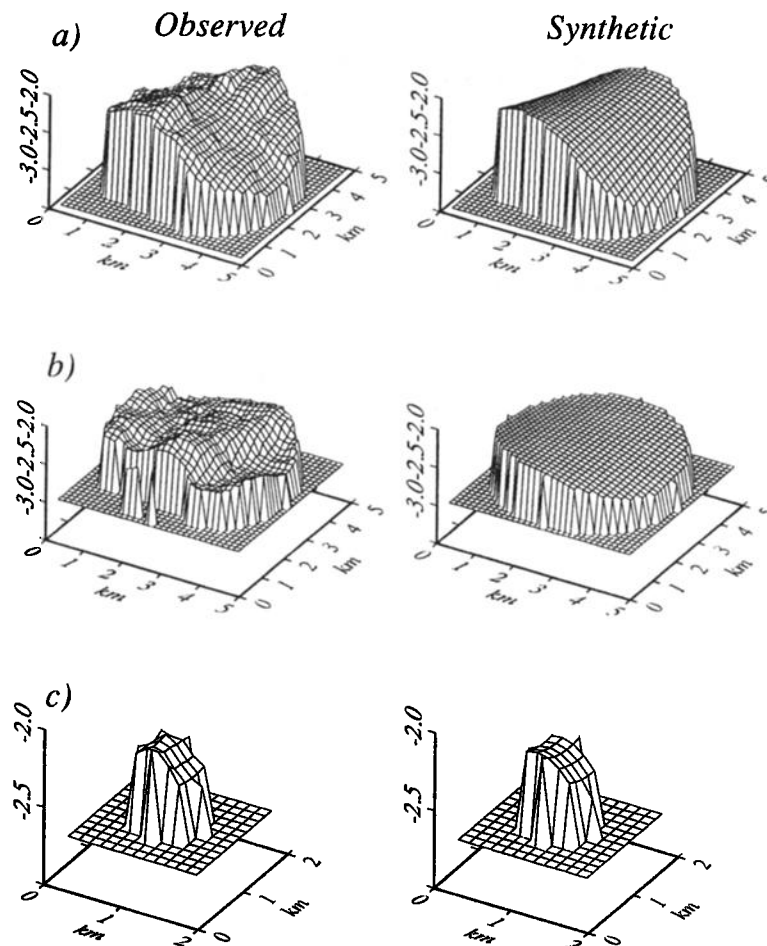

Fig. 2. Illustration of curvature measurement. Each row contains observed topography on the left and the best fitting quadratic on the right. (*a*) Sample of topography containing a large topographic ridge; radius of circular window is 15 grid points, or 2.2 km. Best fitting quadratic surface accurately models overall shape of the ridge; the sharp concave-down curvature of this surface indicates the presence of a significant topographic feature. (*b*) In a different region, topography within 2.2-km-radius window contains several smaller-scale ridges; these are not matched well by the single quadratic surface. (*c*) Smaller window radius (Three grid points, or 0.45 km) singles out an individual ridge from the topographic sample in Figure 2b, allowing the quadratic surface to accurately record the sharpness of the peak. Varying the radius of the window used in the quadratic fitting thus allows the spatial scale of the topographic ridges to be measured.

1976; *Searle and Laughton*, 1977]. At the 0.45 km-scale the curvature threshold used in Figure 1b effectively flags the well-developed large-throw abyssal hill lineations outside the median valley but flags few features within the valley, demonstrating that the abyssal hill lineations in this region develop mostly at the median valley walls and not at the volcanic ridge.

3. APPLICATION TO THE MID-ATLANTIC RIDGE

In the next three sections we discuss variations in the pattern of faulting observed along the MAR, some possi-

ble mechanisms that may underlie the variations in fault spacing, and the evolution of the rift valley into the rift mountains.

3.1. Data Example

A representative section of the Sea Beam data is shown in Plate 1. The sample spans a range of tectonic environments and topographic features, and extends from the center to the southern end of a segment associated with a significant residual mantle Bouguer anomaly (RMBA) low. At the center of the segment (top of Plate 1) the RMBA is strongly
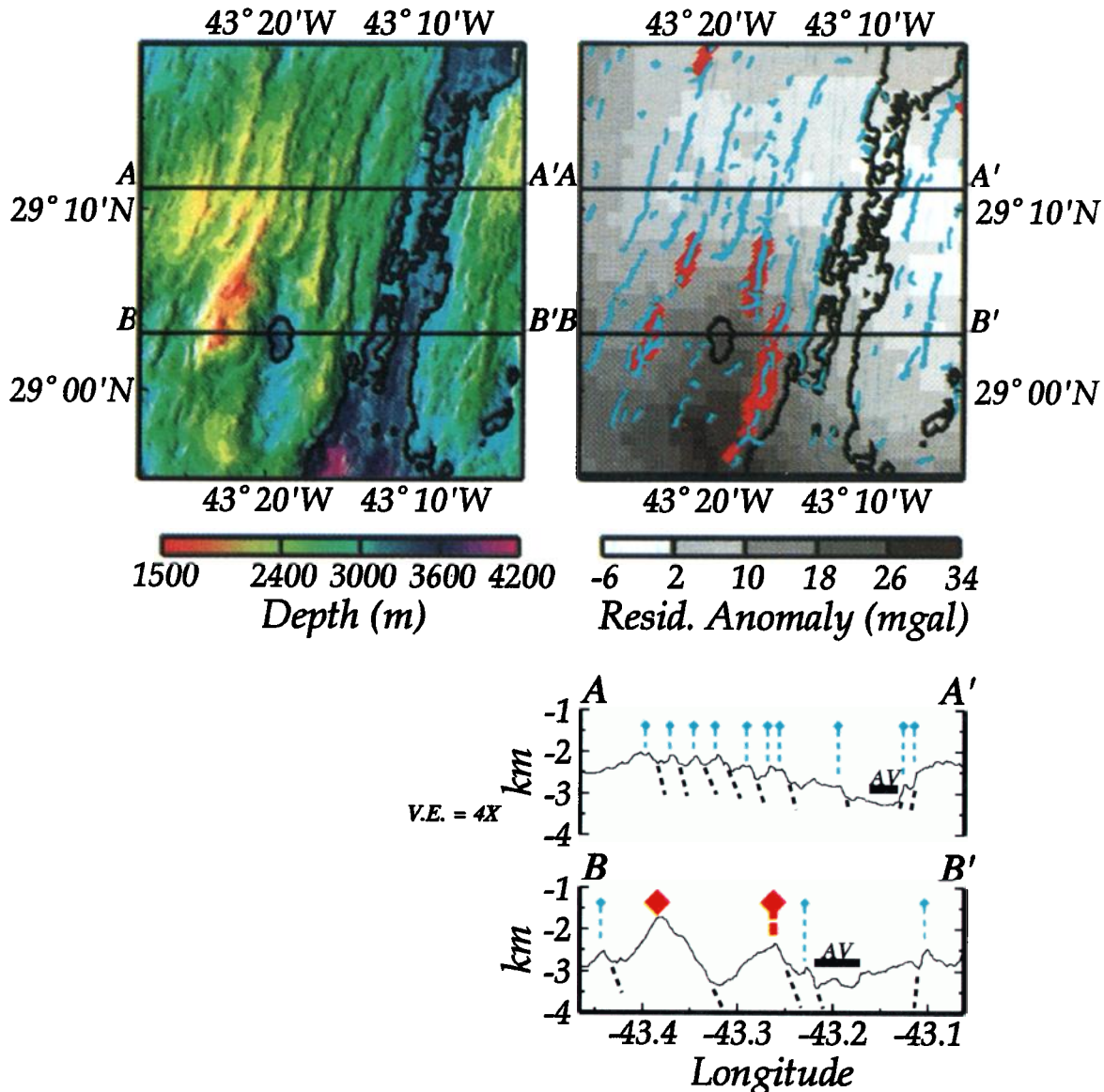

Plate 1. Topographic sample showing application of analysis method; sample is same as in Figure 1. (top left) Shaded relief map (Sun from northwest) of bathymetric sample that includes the median valley, roughly defined by the 3200-m contour (black contour) and a portion of the rift mountains. Profile A-A' samples the center of this ridge segment; B-B' samples near the end of the segment. Topography data are gridded at a 150-m spacing. (top right) Relation between scarps and residual mantle Bouguer anomaly (RMBA) [*Lin et al.*, 1990]. Blue symbols are scarps mapped using a window radius of 0.45 km, chosen to highlight the smallest scarps seen in the data; red symbols are 2.2-km-radius window highlights exclusively the largest scarps and similar large features. Gray shades are RMBA gravity field; 3200-m contour is repeated. (bottom right) Cross section and interpretation of the two profiles A-A' and B-B'; locations of small and large-scale fault corners are indicated. "AV" indicates location and width of 3200-m contour, indicating axial valley. Nearly all the rugged topographic ridges are associated with normal fault scarps, as identified by their sharp edges; these only form starting at the edges of the rift walls. Neovolcanic ridge within median valley [*Sempéré et al.*, 1990; *Smith and Cann*, 1990] does not create any significant highlighted edges. See Plate 2 for location. From *Shaw* [1992].

negative indicating thick crust or elevated mantle temperatures; toward the end of the segment (bottom of figure) the RMBA values are higher, the crust is inferred to be thinner, and a diminished supply of melt is expected [Lin et al., 1990]. The vertical relief between the axial valley and rift mountains in this region is about 1.5 km; the 3200-m contour is drawn to approximately delineate the axial valley. The rift valley is relatively narrow and shallow near the segment center and deeper and wider toward the end.

A series of pronounced, narrow axis-parallel topographic ridges, spaced 1 to 5 km apart, is present in the bathymetry. These ridges begin to develop at the rift valley walls and can be identified across the rift mountains and into the Atlantic abyssal hill terrain; the ridges are largely absent on the median valley floor. Individual ridges are continuous along-strike as much as 40 km and thus represent actual units even though smaller faults that are not resolved by the Sea Beam system are almost certainly present [e.g., Macdonald and Luyendyk, 1977].

Two topographic cross sections, both cutting through the axial valley and rift mountains, are shown at the bottom of Plate 1. Profile A-A' is near the center of this ridge segment where the axial valley is shallow and narrow. Here the abyssal hills are angular in cross section with vertical relief of 200–400 m and a horizontal spacing of approximately 2.5 km; we interpret the angular blocks as elevated foot walls of normal faults. Profile B-B' cuts through the axial valley and rift mountains closer to the end of the segment; here the abyssal hills have a vertical relief exceeding one km and separation approaching 9 km.

The surface expression of faults created near a volcanic center may not necessarily reflect the actual vertical displacement across the faults at depth because of the role of volcanism: as the fault builds up displacement over many slip cycles the hanging wall could be partially filled by fresh volcanics. In such a case, the surface fault displacement would be continuously partially buried and would appear smaller than the actual displacement across the fault at depth. If, in addition, volcanism is more prevalent toward segment centers as a consequence of focused upwelling [Lin et al., 1990], faults near segment centers could appear to have smaller throws than those toward segment ends for this reason. However, the differences between profiles A-A' and B-B' in Plate 1 cannot be entirely explained in this manner because the fault spacing (2.5 km in A-A' versus 9 km in B-B') varies considerably as well as the apparent throw. This difference is instead consistent with the idea that the lithosphere is weaker toward the segment centers than toward the ends and cannot support the large stresses necessary to produce large-throw faults seen toward segment ends. Similar along-axis differences in faults and fissures were observed at the Endeavour Ridge by Barone and Ryan [1988]. In addition to these differences in throw and spacing, the faults close to the segment center (A-A') tend to be long and linear, whereas those nearer a segment end (B-B') tend to be shorter and more curved [Shaw, 1992], reflecting the behavior of the active faults in the rift valley [Sempéré et al., 1990, 1993].

Plate 2 illustrates the relation between the abyssal hill character, ridge segmentation, and the RMBA field over the region 28°N and 29°30'N. Shaw [1992] suggested that the coincidence of the large faults with thin crust inferred from the RMBA field over the region 28°N and 30°30'N provided evidence that the faults, with vertical offsets exceeding 1 km,

are capable of producing significant local crustal thinning as well as a local topographic expression. The penetration of the crust by large near-ridge faults has also been suggested from analysis of earthquakes associated with slow spreading ridges [Bergman and Solomon, 1984; Bratt et al., 1985; Toomey et al., 1985; Huang and Solomon, 1988; Kong et al., 1992].

This correlation is apparent in Plate 1, where associated with the large-throw faults in profile B-B' is a large topographic rise and valley and a significant local maximum in the RMBA, seen as the dark gray shades in the Plate 1 that were interpreted as probable locations of thin crust [Lin et al., 1990].

Plate 2 is plotted so the relation between the abyssal hill texture, the ridge segmentation, and the RMBA field is clearly visible. The style of faulting, both within the median valley and preserved in the rift mountains, is closely related to the ridge segmentation. Toward segment centers the most prevalent faults have relatively small throws and spacings and have flagged curvature expressions only at the 0.45-km scale (Plate 2, right). In plan view these flagged loci are linear and continuous along-strike for as much as 40 km; the ridges are spaced 1–2 km apart and have vertical displacements of 0.2–0.6 km. Toward the segment ends the patterns are more complex; in this region a population of large fault blocks is prevalent, often flagged by both windows but sometimes only flagged by the larger (2.2 km) window. Here the faults generally have larger vertical displacements (0.8–1.2 km) and horizontal spacing (4–8 km) and are shorter (5–10 km) and are less linear than toward segment centers. This analysis is limited by the resolution of the Sea Beam bathymetric data and does not address the behavior of smaller, unresolved fissures and faults.

Nearly all of the lineations flagged with the 0.45 and 2.2-km-radius windows fall outside the rift valley, defined by the 3200-m contour. The rift valley floor is composed primarily of constructional volcanic piles and mounds [Smith and Cann, 1990, 1992]. If these mounds were the mechanism responsible for the abyssal hill topography, then we would expect the flagged lineations to appear within the rift valley floor, including the AVR itself. Because the onset of these lineations is delayed until the rift valley walls, we conclude that the growth of normal faults at the edges of the rift valley is the primary mechanism responsible for Atlantic abyssal hill topography in these data.

The correlation between the large-throw faults toward segment ends with high RMBA values suggests that these large faults contribute to the crustal thinning in these regions [Macdonald, 1982; Shaw, 1992]. In addition to this mechanism, the availability of melt toward segment centers from inferred mantle upwelling is also likely to create a thicker crustal section here than at segment ends; the heat released during this process brings the isotherms shallower, thinning the brittle plate toward segment centers. Normal faults active in this weak region could not develop large throws because new faults readily break through nearby plate. Toward segment ends, with less melt available, the lithospheric plate is likely to be thicker and stronger. Faults here would develop larger throws before new faults are generated, resulting in a larger fault spacing. Superimposed on this general pattern of thin crust occurring toward segment ends will be the characteristic asymmetric patterns related to inside vs. outside corners at both transform and nontransform offsets [Dick, 1981; Karson and Dick, 1983;
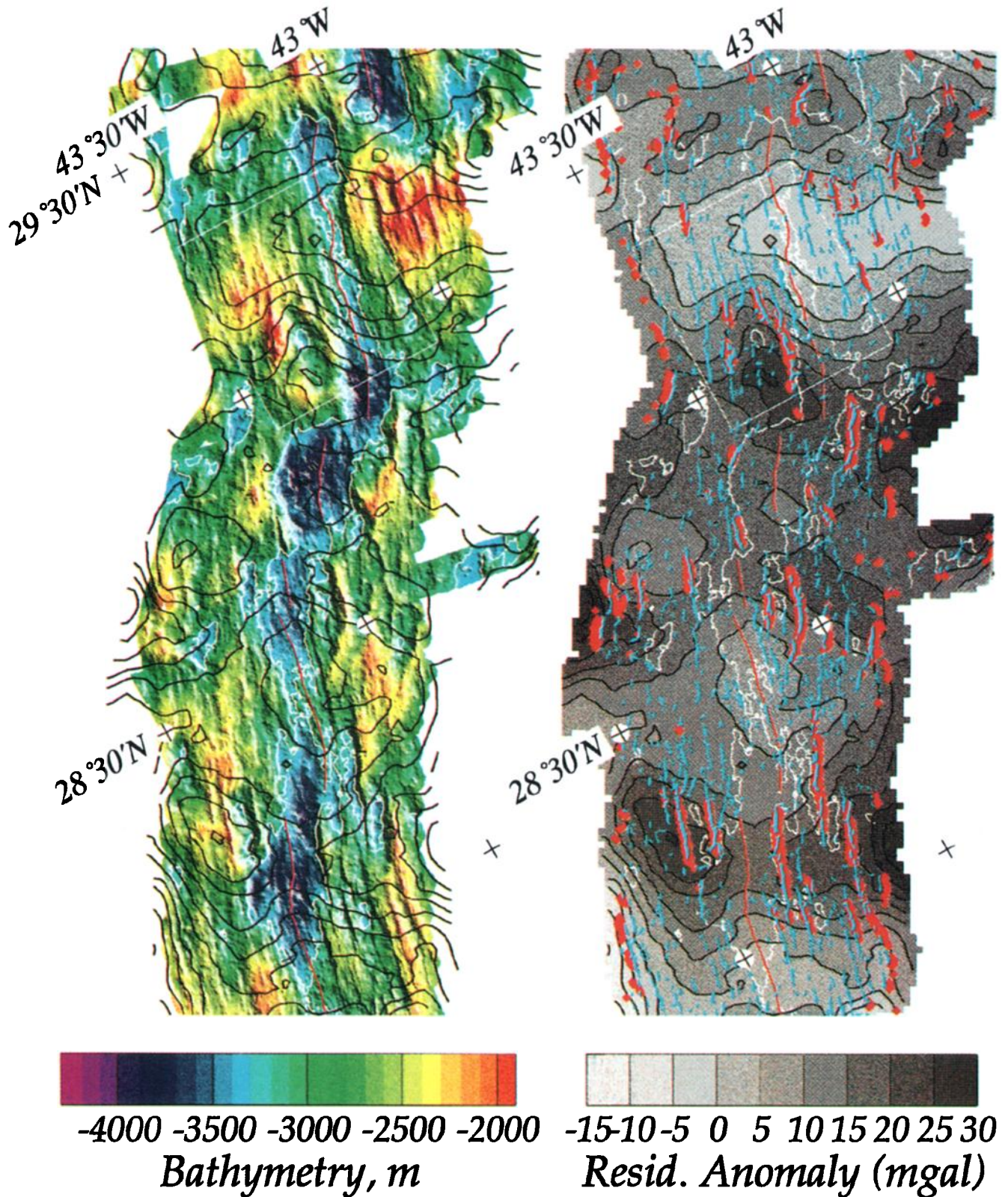
Plate 2. Relation between abyssal hill character, ridge segmentation, and the RMBA gravity field over the analysis region. (left) Shaded-relief view of bathymetry, with illumination from the east. Yellow and red shades correspond to shallow topography; 3200-m contour enclosing dark blue shades indicates the rough location of median valley. The illumination highlights sharp lineations characteristic of abyssal mountains and Atlantic abyssal hill terrain. Rectangle shows location of data sample in Plate 1. contours of RMBA gravity [*Lin et al.,* 1990] are superimposed. (right) RMBA (gray shades) with locations of large curvature, interpreted as faults (symbols) superimposed. Light shades indicate RMBA lows, inferred centers of mantle upwelling and thick crust; dark gray indicates thin crust. Blue symbols are locations of fault corners found using the 0.45-km-radius analysis window; red symbols are corners found with 2.2-km-radius window. This presentation emphasizes the correlation of abyssal hill texture with the RMBA field: rugged lineations associated with clusters of large-throw faults occur predominantly over RMBA highs.

Kuo et al., 1984; *Severinghaus and Macdonald*, 1988; *Brown and Karson*, 1988; *Dick et al.*, 1991; *Blackman and Forsyth*, 1991].

3.2. Inward and Outward faults

Three hypotheses have been proposed to explain the processes through which the relief of the rift valley and the regional slope of the valley walls are subdued or disappear in the rift mountains. In one, the crust rotates as it passes over the rift mountains, so that the regional slopes (5°-9°) in the valley walls are rotated to approximately horizontal. In a second the rift valley relief is decreased by reverse faulting on existing faults. A third hypothesis is that new, outward facing normal faults appear in the rift mountains. The underlying forces controlling these surface processes are described by several models of the dynamics of slow spreading centers [*Harrison*, 1974; *Harrison and Stieltjes*, 1977; *Macdonald and Luyendyk*, 1977; *Macdonald and Atwater*, 1978].

Some insight can be gained in these processes by identifying inward and outward facing scarps by examining the relation of the scarp edges with the steep slopes, as in Figure 3. Nearly all the scarps located with the curvature threshold are asymmetric in cross-section, seen in Figure 3 as a tendency for steep slopes to be more prevalent on one side of the crests. In nearly all of the faults highlighted here, the steep slopes cluster on the innermost side of the crests, implying that nearly all the faults are inward dipping. This result appears counter to the third hypothesis mentioned above that calls for new outward facing faults to appear in the rift mountains.

Inward facing normal faults in the rift valley wall environment of slow spreading ridges have been imaged using the GLORIA system [*Searle and Laughton*, 1977; *Laughton and Searle*, 1979]; however, the apparent absence of systematic outward faulting at these Sea Beam scales reinforces the idea that the outward faulting model suggested by *Macdonald and Luyendyk* [1977] and *Macdonald and Atwater* [1978] is not the primary mechanism for eliminating the steep walls of the rift valley [*Macdonald*, 1982]. The Sea Beam data in this study extend approximately 30 km to either side of the

volcanic axis, so the transition into the rift mountain environment should be well developed. Here we hypothesize that any outward faulting occurs on a scale too small to appear on the Sea Beam records (similar to the small scale inward facing scarps only visible on Deep Tow records [*Macdonald and Luyendyk*, 1977]) and constitutes a relatively insignificant process in the formation of topography. We suggest that the transition from rift valley to rift mountains can be accomplished through the cumulative rotational effects of faults as they occur at the ridge axis.

4. MODELS

Because normal faults are the passive response of the lithosphere to horizontal stresses, the along-axis variations in scarp trends, spacing, and throw evident in Plate 2 must arise either from changes in the stress field, the underlying lithospheric strength, or the underlying fault geometry. Here we investigate two different physical mechanisms that may be active in the MAR environment and the possible effects on scarp spacing. The models differ primarily in whether nearby faults are assumed to be active simultaneously or in sequence.

4.1. Sequential Faulting Model

In this section we investigate a conceptual model in which only one fault is active at a time. This active fault grows to a maximum size and then stops growing while fault activity jumps inward to a new nucleation site where the next active fault begins to grow [*Bicknell et al.*, 1988].

We apply the flexural model of *Forsyth* [1992] to examine several variables that might control fault spacing and throw. Forsyth modeled the behavior of the lithosphere at a normal fault as two cantilevers (broken plates). The stresses involved in fault extension will depend upon several key parameters: the coefficient of friction μ across the fault, the elastic plate thickness H, and the angle θ from horizontal of the fault. Additional parameters that enter the model are cohesion c across an unbroken fault, the density contrast between the mantle and water column $\Delta\rho$, as well as Young's modulus E and Poisson's ratio ν of the elastic layer (see Table 1 for symbol definitions and assumed values).
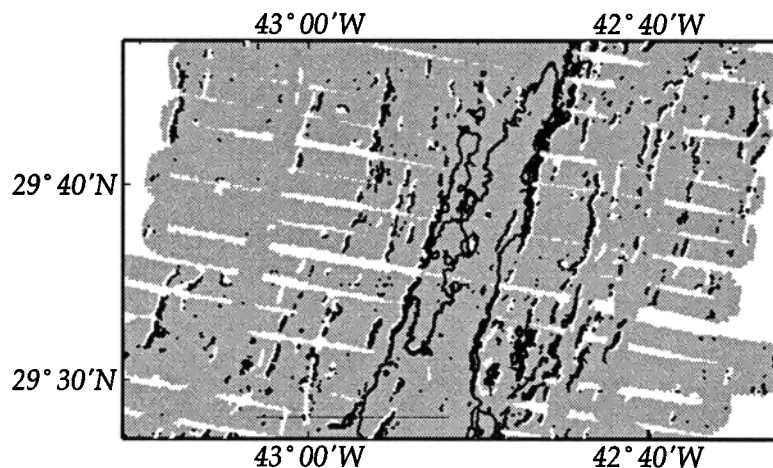

Fig. 3. Illustration of inward and outward facing faults, identified by plotting locations of sharp fault corners (light symbols) with locations of large topographic slope values (dark symbols); 3200-m contour indicating median valley is also plotted; data coverage indicated by medium gray. Nearly all the steep slopes occur inward of the corners, indicating a predominance of inward facing faults. New, outward facing faults do not appear to be formed in the rift mountains.

TABLE 1. Model Parameters

Parameter	Units	Value	Definition
c	Pa	20×10^6	cohesion across unbroken fault
f		0.2	fraction of tectonic extension from faulting
g	m s^{-2}	9.8	gravitational acceleration
k_e	kg m^{-1} s^{-2}		kernal used in σ_e
s	m		fault spacing
E	Pa	0.7×10^{11}	Young's modulus of lithosphere
H	m		brittle plate thickness
θ	deg		angle of fault, measured from horizontal
λ	m		flexural wavelength
μ		0.65	coefficient of friction on fault
ν		0.25	Poisson's ratio of lithosphere
$\Delta\rho$	kg m^{-3}	2300	density contrast between mantle and water
σ_c	Pa		stress necessary to overcome cohesion on fault
σ_e	Pa		stress necessary to cause fault flexure
σ_f	Pa		stress necessary to overcome fault friction
σ_R	Pa		total regional stress needed to activate existing fault
Δx	m		horizontal displacement of fault (heave)
Δx_{max}	m		maximum fault heave before new fault breaks

We define σ_f, σ_c, and σ_e, the stresses associated with friction, cohesion, and elastic flexure, respectively, following the formulation of Forsyth [1992],

$$\sigma_f(\mu, H, \theta) = \frac{\mu \, \Delta\rho \, gH/2}{\mu \sin^2 \theta + \sin \theta \cos \theta} \quad (3)$$

$$\sigma_c(\mu, \theta) = \frac{c}{\mu \sin^2 \theta + \sin \theta \cos \theta} \quad (4)$$

$$\sigma_e(H, \theta) = k_e(H, \theta) \, \Delta x \quad (5)$$

$$k_e(H, \theta) = \frac{[E(\Delta\rho \, gH)^3/3(1 - \nu^2)]^{1/4} \tan^2 \theta}{4H} \; ; \quad (6)$$

the elastic stress σ_e is thus linearly related to the extension (heave) of the fault Δx through the kernal k_e. The cohesional stress σ_c is assumed to be present only in unbroken lithosphere and drop to zero once a fault breaks; the coefficient of friction on the fault is assumed constant. As extension continues the flexural stress σ_f grows linearly with the extension, or heave Δx across the fault. A new fault will thus break through the lithosphere when the total stresses necessary to activate the existing fault become equal to the minimum stresses needed to break a new fault.

Assuming the stress necessary to break a new fault is the sum of frictional stress plus cohesion, $\sigma_f + \sigma_c$, the stresses necessary to displace an existing fault already extended by an amount Δx is modeled as frictional stress plus the elastic stress, $\sigma_f + \sigma_e$. The maximum fault heave possible before a fault breaks at a new location is thus

$$\Delta x_{max} =$$
$$\frac{\sigma_f(\mu_{new}, H, \theta_{new}) + \sigma_c(\mu_{new}, \theta_{new}) - \sigma_f(\mu_{old}, H, \theta_{old})}{k_e(H, \theta_{old})} \quad (7)$$

where subscripts "old" and "new" refer to an existing and new fault, respectively, in order to allow friction or fault angle to vary as a fault is extended.

In the ocean ridge environment, new faults are likely to form preferentially near the rift valley, where the lithosphere is thinnest [e.g., Searle, 1984; Bicknell et al., 1988; Carbotte and Macdonald, 1990]. For simplicity, we assume that new faults form at a fixed distance from the volcanic axis in order to investigate the overall properties of this model; more complicated models could easily be devised, however. As extension across the fault grows, the fault also migrates away from the spreading center as dikes are intruded at the axis.

We assume that a fixed fraction of plate extension occurs through fault slip with the rest occurring through dike injection; this ratio will determine the relation between fault spacing and fault heave $s = \Delta x/f$, where s is fault spacing, Δx is fault heave, and f is the fraction of extension occurring as faulting. This relation is significant because it is much easier to infer fault scarp spacing from topographic data than fault heave, owing to the limited spatial resolution of the Sea Beam footprint. Macdonald and Luyendyk [1977] estimated $f \approx 0.18$ for the MAR; Bicknell et al. [1988] estimate $f \approx 0.05$ on the East Pacific Rise near 19°S, and Solomon et al. [1988] estimate f to be 0.1–0.2 from a study of rates of global ocean ridge seismic moment release.

Results of this sequential faulting model are illustrated in Figure 4, which shows the span of fault heave Δx_{max} predicted for a range of lithospheric thickness and fault angle. The fault heave increases with increasing brittle plate thickness; this is expected to occur toward ridge segment ends and away from mantle upwelling foci. Ridge segment ends are also the region where large fault separations are observed. The angle of the fault is an additional parameter which affects the fault spacing: for a steep fault angle the required stress builds up quickly with horizontal displacement and the fault cannot accommodate as much displacement as a shallower-angle fault before reaching the breaking stress [Forsyth, 1992].

Point "a" in Figure 4 represents a series of faults with $\theta = 50°$ in an elastic lithosphere 10 km thick. With these parameters the flexural model predicts a characteristic fault heave of 1.5 km. This heave roughly corresponds to that observed near the end of a segment; toward the centers of segments the heave is significantly smaller. In order to decrease the fault heave, two options are available with this model: the elastic thickness can be decreased, or the fault angle may be increased (steepened). Point "b" accomplishes a decrease in heave by a factor of approximately 2 (to 0.8 km) by a fourfold decrease in elastic thickness, to 2.5 km. This large decrease in lithospheric strength might occur over an active zone of mantle upwelling. Alternatively, the elastic thickness could remain the same, but the fault angle could increase to 60°, as indicated in point "c", which yields the same fault heave. Using a value $f = 0.2$ for the fraction of extension accommodated through faulting [Solomon et al., 1988], fault heaves of 1.5 km and 0.8 km yield fault spacings
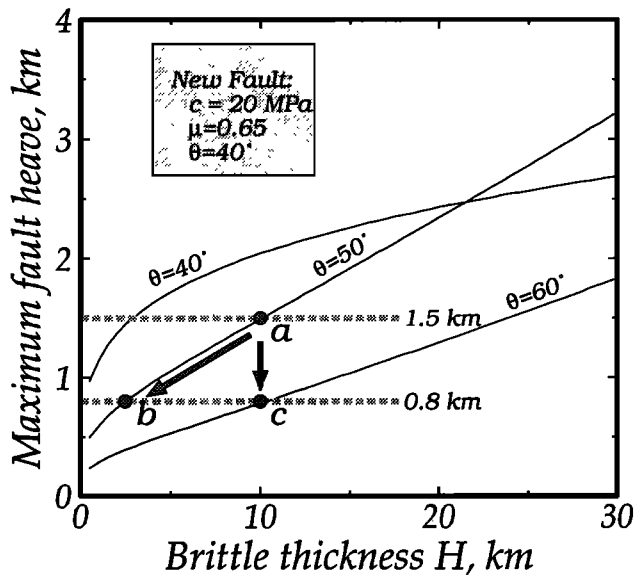
Fig. 4. Theoretical curves showing how maximum fault heave Δx_{max} varies with elastic plate thickness H, fault angle θ, and coefficient of friction μ. Maximum heave on a given fault occurs when the stress necessary to create further fault displacement reaches the breaking stress for the formation of a new fault. To avoid varying many parameters simultaneously, the new fault is assumed to occur at a constant angle $\theta = 40°$ with coefficient of friction $\mu = 0.65$. The maximum heave increases with increasing lithospheric thickness, decreasing fault angle, and also decreasing friction (not shown). Calculations are based on model by Forsyth [1992]. With this model, setting $H = 10$ km and $\theta = 50°$ yields $\Delta x_{max} = 1.5$ km (point "a"), as might be observed toward the ends of a segment. Smaller heave faults such as occur toward ridge segment centers might arise either from a reduction in elastic plate thickness H (point "b") or by changing the fault angle to $\theta = 60°$ (point "c").

of 7.5 km and 4 km, respectively. It is noteworthy that on the basis of fault heave or spacing alone, points "b" and "c" cannot be easily distinguished.

Although the great majority of normal fault scarps detectable with Sea Beam are inward dipping, this finding is consistent with the presence of a steady state rift valley, given an understanding of the flexural response of the lithosphere to normal faults. Horizontal extension along a dipping normal fault causes the lithosphere on either side to flex, causing a rotational effect [Buck, 1988; Weissel and Karner, 1989; Forsyth, 1992]. The flexural wavelength of the lithosphere is a function of the effective lithospheric thickness; the larger this wavelength is, the more seafloor to either side of the fault will experience a flexural rotation. In particular, if the flexural wavelength is greater than the fault spacing, the activation of new normal faults at the edge of the rift valley will cause adjacent fault blocks to rotate. If normal faulting occurs in a narrow zone toward the edge of the axial valley, then each fault block will accumulate a net rotation from the new faults as it moves away from the ridge crest before finally moving sufficiently far from the active fault zone that it is no longer affected by the new faulting.

A simple model exploring the consequences of this idea is shown in Figure 5 to model the response of the lithosphere to a sequence of normal faults. The model employs an constant thickness elastic lithosphere overlying a fluid, which approximates a Maxwell viscoelastic half-space at large time scales

[Weissel and Karner, 1989]. This simulation only attempts to model one half of the axial topography, rather than the full symmetric axial valley and rift mountains; however, the overall form of the faulted profile bears a strong resemblance to actual MAR topography. In particular, the transition in the regional slope from rift valley to rift mountains is accomplished without either reverse faulting along existing faults or new outward facing faults forming in the rift mountains.

Figure 6 illustrates the differences between models represented between geometries "a," "b," and "c" in Figure 4. Geometry "a" is illustrated in Figure 6a: a nominal elastic
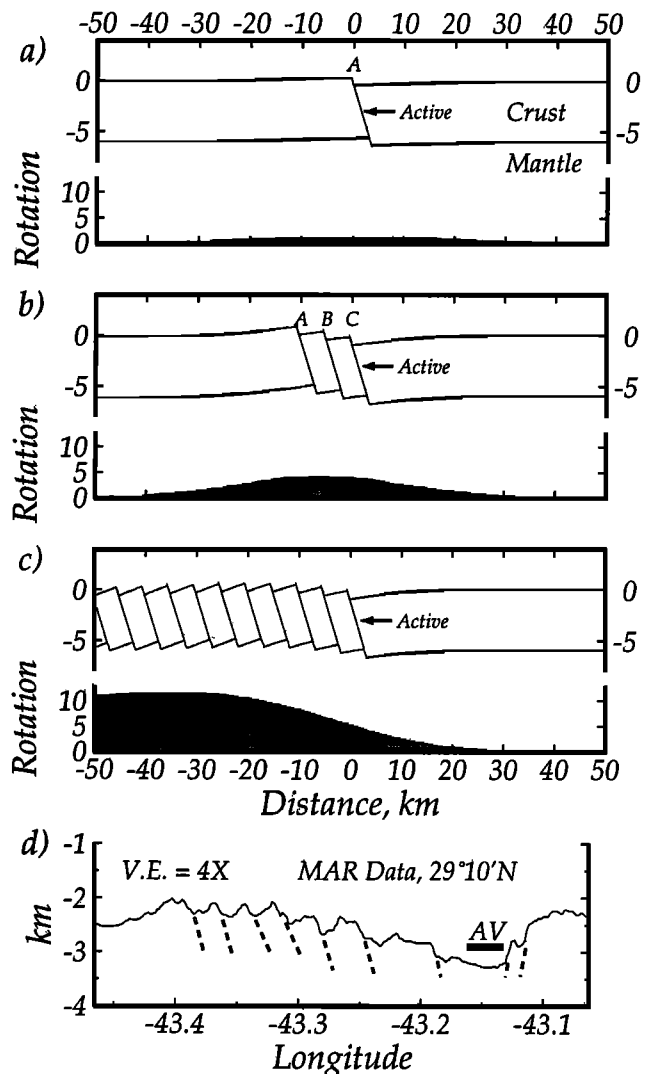

Fig. 5. Illustration showing how cumulative flexure resulting from a sequence of normal faults can produce a topographic profile resembling the rift valley walls and rift mountains. (a) Flexure from a single fault ("A") produces topography on basement and Moho; calculations follow the continuous plate model [Weissel and Karner, 1989] which assumes that the plate retains its elastic strength during faulting. Distances in kilometers; 2× vertical exaggeration; rotation in degrees. (b) Subsequent faulting on two additional faults produces flexural rotation on now inactive fault "A". Reference frame is centered on the currently active fault. (c) After a large number of normal faults have formed, a flexural bulge develops over the faulted section of lithosphere; this bulge arises from the cumulative rotation of the sequence of faults. The resulting structure resembles one half of a median valley, where individual normal faults produce the rift wall and rift mountains. (d) Median valley topography, repeated from profile A-A' of Plate 1.
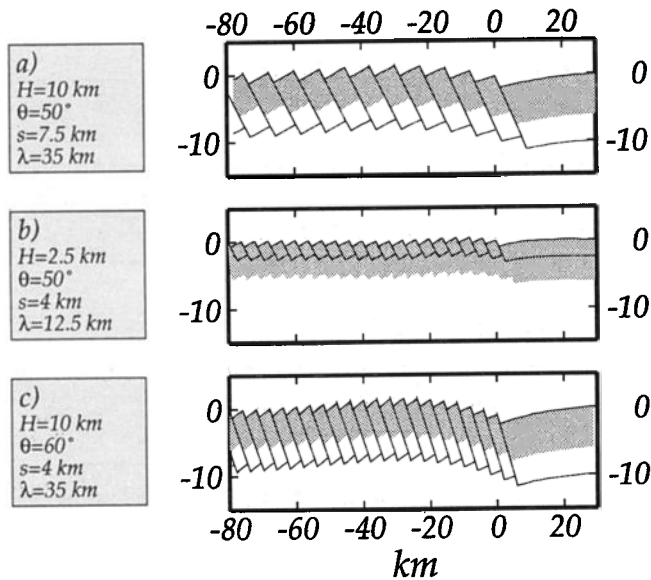
a)
H=10 km
θ=50°
s=7.5 km
λ=35 km

b)
H=2.5 km
θ=50°
s=4 km
λ=12.5 km

c)
H=10 km
θ=60°
s=4 km
λ=35 km

Fig. 6. Portrayal of the differing flexural response to multiple faults as elastic plate thickness H or angle θ varies. Figures 6a, 6b, and 6c illustrate points "a," "b," and "c" in Figure 4, assuming a ratio $f = 0.2$ (the ratio of extension through faults to extension through dikes). Fault spacing s is related to maximum fault heave Δx_{max} by $s = f\,\Delta x_{max}$. Although the geometries in Figures 6b and 6c have the same fault spacing, the amplitude and wavelength of the flexural bulge in the faulted region vary substantially. Shaded region represents crust (initially 6 km thick).

plate thickness of 10 km and fault angle of 50° produces a fault spacing of 7.5 km. Although both geometries "b" and "c" have fault spacings of 4 km (Figures 6b and 6c), in geometry "b" the fault angle remains 50°, but the plate thickness has been reduced to 2.5 km. In "c" the elastic thickness remains 10 km, but the fault angle has changed to 60°, thus decreasing the fault spacing.

Importantly, the flexural differences between the geometries may provide the necessary clues to distinguish them, even though the fault spacings may not be sufficient. For example, although the fault spacings in "b" and "c" are the same, the differences in flexural relief and wavelengths reflect the large differences in plate thickness H.

4.2. Necking Instability Model

We next consider a model that represents the opposite end of the spectrum from the previous one. Rather than assuming that each fault grows to its full size independently of the growth of nearby faults, we now consider the possibility that multiple faults may be actively growing simultaneously. In such a situation one mechanism that will influence fault spacing is illustrated in Figure 7, which shows the state of stress induced in an infinite elastic half-space from a normal fault dipping at 45°. Shades of gray indicate levels of compression or dilatation, computed using a boundary elements formulation that follows the method of *Crouch and Starfield* [1983] and *King and Ellis* [1990]. The shades show how the presence of a fault significantly affects the state of stress in the surrounding lithosphere and will influence the location of future faults: a potential new fault will preferentially grow in a region that is under tension (dark regions) rather than in regions in compression (white). The surficial gray region to the left of the fault is the likeliest zone of new fault growth. This pattern of dilatation is scale invariant, so an increase by a factor of 2 of fault penetration from that shown in Figure 7 will double the distance of the gray area from the fault. Variations in the lithosphere thickness will therefore be significant because an increased thickness will increase the natural spacing of faults. From this argument, a variation by a factor of 3 in fault spacing as seen in Plate 2 would correspond into a factor of 3 variation in brittle thickness.

Because each fault relieves stresses as it grows, it inhibits the growth of nearby faults and causes a characteristic fault spacing. This type of interaction between faults would occur in a region of necking instability involving deformation over an extended area, and drive a feedback mechanism that would act to regulate the size and spacing of nearby faults [*Zuber et al.*, 1986].

5. DISCUSSION

The identification of seafloor scarps allows us to address a number of issues regarding processes that are active at the MAR rift environment: First, the analysis clarifies the relative importance of faulting and volcanism in the creation of Atlantic abyssal hill terrain and in doing so identifies the
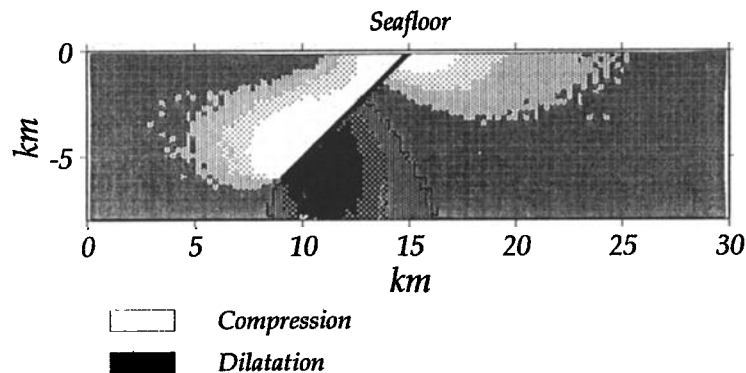

Seafloor

□ Compression
■ Dilatation

Fig. 7. Boundary element visualization of crustal deformation near a normal fault. The results are shown of dilatation produced by 1 m of slip on a 8-km-wide fault dipping 45°. A uniform stress drop condition is assumed for the fault plane, resulting in a quadratic decrease of fault slip toward the fault tip at depth. The fault creates dilatation areas (dark), in which further faulting and magma intrusion are likely to occur. The surficial gray region to the left of the fault is the likeliest zone of new fault growth.

locations within the rift environment where each process is active. The picture that emerges of the rift environment is that the active volcanism and faulting occur in the immediate vicinity of the rift valley, as envisioned by workers making direct observations from submersibles [e.g., *ARCYANA*, 1975].

Second, the identification of scarps allows us to study their along-axis variations; these are closely related to their locations within the ridge segments, the residual mantle Bouguer field, and mantle upwelling. The RMBA anomaly in this region can arise from some combination of low-density mantle or thick crust [*Lin et al.*, 1990]. We have shown that the observed fault patterns, e.g., numerous small-throw faults occurring toward segment centers, are consistent with shallower isotherms and weaker lithosphere in these areas that would result from the crystallization of a thicker crustal column here. This apparent sensitivity of fault parameters to the thermal structure of the lithosphere can be exploited to draw inferences not only about the present-day rift environment but also about the evolution in time of the thermal structure. Abyssal hill character might prove a useful parameter to consider in addition to bathymetric depth and the RMBA field when considering trails of ridge offsets preserved off-axis [e.g., *Johnson and Vogt*, 1973; *Rona et al.*, 1976; *Schouten et al.*, 1987].

Third, the identification of individual faults and their directionality on a regional basis gives us insights into how the rift valley floor evolves into the steep valley walls and then the rugged rift mountains. The predominance of inward facing faults shows that large outward facing faults are not systematically created in the rift mountains. Rather, the evolution of the rift valley into rift mountains and then abyssal hill terrain may be accomplished primarily through flexural effects. We envision that the evolution of the rift valley floor to rift mountains occurs as the innermost active normal fault at the rift wall stops its movement, transferring extension to a new weakness site within the valley floor and initiating the growth of a new normal fault. The valley floor trapped between these two faults is thrust upward with displacement of the new fault and eventually rotated as it passes into the rift mountains.

The observed variations with position within a ridge segment in fault spacing and character, which influences the abyssal hill fabric off-axis, are related to the width and relief of the axial valley [*Shaw*, 1992; *Sempéré et al.*, 1993]. We have examined two different physical mechanisms that may explain the variations in faulting. The first mechanism assumes faults are active individually; their spacing thus reflects the distance the fault is carried off-axis before the next fault is initiated. This distance in turn is controlled by the elastic thickness, as illustrated in Figure 6; here, differences in the flexural wavelength and elastic thickness create axial valley profiles that differ greatly in appearance.

An alternative mechanism considers several faults that develop simultaneously. In this scenario the interfault spacing is determined through a feedback mechanism between the faults as they grow. The number of simultaneously active faults would be determined by the width of an extended zone of deformation; the wider this zone, the more faults that would be active at any time.

We hypothesize that this second mechanism may be active toward segment centers where the abyssal hill texture is remarkably homogeneous, reflecting a near uniformity of spacing and throw of normal faults. This homogeneity suggests that such a feedback mechanism might be in effect, regulating the spacing and throw of nearby faults. Toward the ends of ridge segments faults would grow independently of one another and thus would be more variable in spacing and throw.

This hypothesis is supported by the correlation of the homogeneous abyssal hill zone with a narrow, lower-relief rift valley that develops most frequently at segment centers [*Sempéré et al.*, 1993]. The physical model proposed by *Chen and Morgan* [1990] associates a pronounced rift valley with a narrow zone of lithosphere failure such as in the slow spreading Atlantic and no rift valley with an extended zone of deformation owing to a wide melt-related decoupling zone in the fast spreading Pacific. As a result, changes in ridge character are observed over a range of spreading rates [*Small and Sandwell*, 1989]. Within a single Atlantic ridge segment, an increase in available melt toward the center would then act to increase the size of such a decoupling region, acting to decrease the relief and width of the rift valley.

6. CONCLUSIONS

1. The majority of the abyssal hill lineations analyzed in this study appear to be created through the process of faulting, rather than constructional volcanism. Within the median valley constructional volcanism is the dominant topography-building process; large normal faults develop at the valley walls and constitute the abyssal hill lineations.

2. A pattern of long, linear, small-throw faults with relatively small fault spacing is observed toward segment centers, and the opposite pattern is observed toward segment ends. These observations are consistent with warmer, weaker lithosphere present toward segment centers. Application of a simple flexural model (in which abyssal hills form one hill at a time) suggests that thickening of the lithosphere, shallowing of fault angles, or both toward the segment ends can account for these differences. Alternatively, the faulting regime toward ridge segment centers could be explained with a necking instability model in which several nearby faults grow together, regulating the throw and spacing of individual faults to be relatively uniform.

3. The normal faults mapped in this study are predominantly inward facing, in concordance with evidence from GLORIA surveys and near-axis submersible observations. The directions of faults are probably controlled by the strong thermal gradient near the ridge, creating a preferred direction for faults to propagate. However, the elimination of the rift wall seems not to be accomplished by the formation of new outward faults in the rift mountains at least not in the data analyzed in this study, which extends approximately 30 km to either side of the ridge axis. Rather, a simple multiple-fault flexural model suggests that the flexural rotation associated with normal faulting near the ridge axis is sufficient to remove rift walls and form the rift mountains. This observation would be consistent with the description of inward facing normal faults separating regions of outward tilting seafloor.

REFERENCES

ARCYANA, Transform fault and rift valley from bathyscaph and diving saucer, *Science, 190,* 108–116, 1975.

Ballard, R. D., and T. van Andel, Morphology and tectonics of the inner rift valley at lat 36°50'N on the Mid-Atlantic Ridge, *Geol. Soc. Am. Bull., 88,* 507–530, 1977.

Barone, A. M. and W. B. F. Ryan, Along-axis variations within the plate boundary zone of the southern segment of the Endeavour Ridge, *J. Geophys. Res., 93,* 7856–7868, 1988.

Bergman, E. A., and S. C. Solomon, Source mechanisms of earthquakes near mid-ocean ridges from body waveform inversion: Implications for the early evolution of oceanic lithosphere, *J. Geophys. Res., 89,* 11,415–11,441, 1984.

Bicknell, J. D., J.-C. Sempéré, and K. C. Macdonald, Tectonics of a fast spreading center: A Deep-Tow and Sea Beam survey on the East Pacific Rise at 19°30'S, *Mar. Geophys. Res., 9,* 25–46, 1988.

Blackman, D. K., and D. W. Forsyth, Isostatic compensation of tectonic features of the Mid-Atlantic Ridge: 25–27°30'S, *J. Geophys. Res., 96,* 11,741–11,758, 1991.

Bratt, S. R., E. A. Bergman, and S. C. Solomon, Thermoelastic stress: How important as a cause of earthquakes in young oceanic lithosphere?, *J. Geophys. Res., 90,* 10,249–10,260, 1985.

Bronshtein, I. N., and K. A. Semendyayev, *Handbook of Mathematics,* Van Nostrand Reinhold, New York, 1985.

Brown, J. R., and J. A. Karson, Variations in axial processes on the Mid-Atlantic Ridge: The median valley of the MARK area, *Mar. Geophys. Res., 10,* 109–138, 1988.

Buck, W. R., Flexural rotation of normal faults, *Tectonics, 7,* 959–973, 1988.

Carbotte, S. M., and K. C. Macdonald, Causes of variation in fault-facing direction on the ocean floor, *Geology, 18,* 749–752, 1990.

Chen, Y. and W. J. Morgan, Rift valley/no rift valley transition at mid-ocean ridges, *J. Geophys. Res., 95,* 17,571–17,581, 1990.

Crouch, S. L., and A. M. Starfield, *Boundary Element Methods in Solid Mechanics,* Allen Unwin, London, 1983.

Dick, H. J. B., Low angle faulting and steady-state emplacement of plutonic rocks at ridge-transform intersections, *Eos Trans. AGU, 62,* 406, 1981.

Dick, H. J. B., H. Schouten, P. S. Meyer, D. G. Gallo, H. Bergh, R. Tyce, P. Patriat, K. T. M. Johnson, J. Snow, and A. Fisher, Tectonic evolution of the Atlantis II fracture zone, *Proc. Ocean Drill. Program, Sci. Results, 118,* 359–398, 1991.

Forsyth, D. W., Finite extension and low-angle normal faulting, *Geology, 20,* 27–30, 1992.

Harrison, C. G. A., Tectonics of mid-ocean ridges, *Tectonophysics, 22,* 301–310, 1974.

Harrison, C. G. A., and L. Stieltjes, Faulting within the median valley, *Tectonophysics, 38,* 137–144, 1977.

Huang, P. Y., and S. C. Solomon, Centroid depths of mid-ocean ridge earthquakes: Dependence on spreading rate, *J. Geophys. Res., 93,* 13,445–13,477, 1988.

Jackson, J., and D. McKenzie, The geometrical evolution of normal fault systems, *J. Struct. Geol., 5,* 471–482, 1983.

Johnson, G. L., and P. R. Vogt, Mid-Atlantic Ridge from 47° to 51°N, *Geol. Soc. Am. Bull., 84,* 3443–3462, 1973.

Kappel, E. S., and W. B. F. Ryan, Volcanic episodicity and a non-steady state rift valley along northeast Pacific spreading centers: Evidence from Sea MARC I, *J. Geophys. Res., 91,* 13,925–13,940, 1986.

Kappel, E. S., and W. B. F. Ryan, Sea Beam bathymetry along the Mid-Atlantic Ridge provides evidence of abyssal hill formation, *Eos Trans. AGU, 72* (44) Fall Meeting suppl., 467, 1991.

Karson, J. A., and H. J. B. Dick, Tectonics of ridge-transform intersections at the Kane fracture zone, *Mar. Geophys. Res., 6,* 51–98, 1983.

Karson, J. A., and P. A. Rona, Block-tilting, transfer faults, and

structural control of magmatic and hydrothermal processes in the TAG area, Mid-Atlantic Ridge 26°N, *Geol. Soc. Am. Bull., 102,* 1635–1645, 1990.

King, G. C. P., and M. Ellis, The origin of large local uplift in extensional regions, *Nature, 348,* 689–693, 1990.

King, G. C. P., R. S. Stein, and J. B. Rundle, The growth of geological structures by repeated earthquakes, 1, Conceptual framework, *J. Geophys. Res., 93,* 13,307–13,318, 1988.

Kong, L. S. L., R. S. Detrick, P. J. Fox, L. A. Mayer, and W. B. F. Ryan, The morphology and tectonics of the Mark area from Sea Beam and Sea MARC I observations (Mid-Atlantic Ridge 23°N), *Mar. Geophys. Res., 10,* 59–90, 1988.

Kong, L. S. L., S. C. Solomon, and G. M. Purdy, Microearthquake characteristics of a mid-ocean ridge along-axis high, *J. Geophys. Res., 97,* 1659–1685, 1992.

Kuo, B.-Y., W. J. Phipps Morgan, and D. W. Forsyth, Asymmetry in topography of the crestal mountains near a ridge-transform intersection, *Eos Trans. AGU, 65,* 274, 1984.

Laughton, A. S., and J. S. Rusby, Long-range sonar and photographic studies of the median valley in the FAMOUS area of the Mid-Atlantic Ridge near 37°N, *Mar. Geophys. Res., 23,* 279–298, 1975.

Laughton, A. S., and R. C. Searle, Tectonic processes on slow spreading ridges, in *Deep Drilling Results in the Atlantic Ocean: Ocean crust, Maurice Ewing Ser.,* vol. 2, edited by M. Talwani, C. G. Harrison, and D. E. Hayes, pp. 15–32, AGU, Washington, D. C., 1979.

Lin, J., and E. A. Bergman, Rift grabens, seismicity, and volcanic segmentation of the Mid-Atlantic Ridge: Kane to Atlantis fracture zones, *Eos Trans. AGU, 71,* 1572, 1990.

Lin, J., G. M. Purdy, H. Schouten, J.-C. Sempéré, and C. Zervas, Evidence from gravity data for focused magmatic accretion along the Mid-Atlantic Ridge, *Nature, 344,* 627–632, 1990.

Luyendyk, B. P. and K. C. Macdonald, Physiography and structure of the inner floor of the FAMOUS rift valley: Observations with a deep-towed instrument package, *Geol. Soc. Am. Bull., 88,* 648–663, 1977.

Macdonald, K. C., Mid-ocean ridges: Fine scale tectonic, volcanic and hydrothermal processes within the plate boundary zone, *Annu. Rev. Earth Planet. Sci., 10,* 155–190, 1982.

Macdonald, K. C., The crest of the Mid-Atlantic Ridge: Models for crustal generation processes and tectonics, in *The Geology of North America,* vol. M, *The Western North Atlantic Region,* pp. 51–68, Geological Society of America, Boulder Colo., 1986.

Macdonald, K. C., and T. M. Atwater, Evolution of rifted ocean ridges, *Earth Planet. Sci. Lett., 39,* 319–327, 1978.

Macdonald, K. C., and B. P. Luyendyk, Deep-tow studies of the structure of the Mid-Atlantic Ridge crest near lat 37°N, *Geol. Soc. Am. Bull., 88,* 621–636, 1977.

Macdonald, K. C., B. P. Luyendyk, J. D. Mudie, and F. N. Spiess, Near-bottom geophysical study of the Mid-Atlantic Ridge median valley near lat 37°N: Preliminary observations, *Geology, 3,* 211–215, 1975.

Menke, W., *Geophysical Data Analysis: Discrete Inverse Theory,* Academic, San Diego, Calif., 1984.

Needham, H. D. and J. Francheteau, Some characteristics of the rift valley in the Atlantic Ocean near 36°48'N, *Earth Planet. Sci. Lett., 22:* 29–43, 1974.

Pockalny, R. A., R. S. Detrick, and P. J. Fox, Morphology and tectonics of the Kane Fracture Zone from Sea Beam bathymetry data, *J. Geophys. Res., 93,* 3179–3193, 1988.

Purdy, G. M., J.-C. Sempéré, H. Schouten, D. L. DuBois, and R. Goldsmith, Bathymetry of the Mid-Atlantic Ridge, 24°–31°N: A map series, *Mar. Geophys. Res., 12,* 247–252, 1990.

Rona, P. A., R. N. Harbison, and S. A. Bush, Abyssal hills of the eastern central North Atlantic, *Mar. Geol., 16,* 275–292, 1974.

Rona, P. A., R. N. Harbison, B. G. Bassinger, R. B. Scott, and A. J. Nalwalk, Tectonic fabric and hydrothermal activity of Mid-Atlantic Ridge crest (lat 26°N), *Geol. Soc. Am. Bull., 87,* 661–674, 1976.

Rundle, J. B., Viscoelastic-gravitational deformation by a rectangular thrust fault in a layered earth, *J. Geophys. Res., 87,* 7787–7796, 1982.

Schouten, H., H. J. B. Dick, and K. D. Klitgord, Migration of mid-ocean-ridge volcanic segments, *Nature, 326,* 835–839, 1987.

Searle, R. C., GLORIA survey of the East Pacific Rise near 3.5°S: Tectonic and volcanic characteristics of a fast spreading mid-ocean rise, *Tectonophysics, 101,* 319–344, 1984.

Searle, R. C., and A. S. Laughton, Sonar studies of the Mid-Atlantic Ridge and Kurchatov fracture zone, *J. Geophys. Res.*, *82*, 5313–5328, 1977.

Sempéré, J.-C., G. M. Purdy, and H. Schouten, Segmentation of the Mid-Atlantic Ridge between 24°N and 30°40'N, *Nature*, *344*, 427–431 1990.

Sempéré, J.-C., J. Lin, H. S. Brown, H. Schouten, and G. M. Purdy, Segmentation and morphotectonic variations along a slow-spreading center: The Mid-Atlantic Ridge (24°00'N–30°40'N), *Mar. Geophys. Res.*, *15*, 153–200, 1993.

Severinghaus, J. P., and K. C. Macdonald, High inside corners at ridge-transform intersections, *Mar. Geophys. Res.*, *9*, 353–367, 1988.

Shaw, P. R., Ridge segmentation, faulting, and crustal thickness in the Atlantic, *Nature*, *358*, 490–493, 1992.

Shaw, P. R., and D. K. Smith, Statistical methods for describing seafloor topograpy, *Geophys. Res. Lett.*, *14*, 1061–1064, 1987.

Shaw, P. R., and D. K. Smith, Robust description of statistically heterogeneous seafloor topography through its slope distribution, *J. Geophys. Res.*, *95*, 8705–8722, 1990.

Small, C., and D. T. Sandwell, An abrupt change in ridge axis gravity with spreading rate, *J. Geophys. Res.*, *94*, 17,383–17,392, 1989.

Smith, D. K., and J. R. Cann, Hundreds of small volcanoes on the median valley floor of the Mid-Atlantic Ridge at 24–30°N, *Nature*, *348*, 152–155, 1990.

Smith, D. K., and J. R. Cann, The role of seamount volcanism in crustal construction at the Mid-Atlantic Ridge (24°–30°N), *J. Geophys. Res.*, *97*, 1645–1658, 1992.

Smith, D. K., and P. R. Shaw, Using topographic slope distributions to infer seafloor patterns, *IEEE J. Oceanic Eng.*, *14*, 338–347, 1989.

Smith, D. K., J. R. Cann, J. Lin, M. Dougherty, S. Spencer, C. Macleod, J. Keeton, E. MacAllister, R. Pascoe, B. Brooks, and S. Garland, TOBI Deep-tow side-scan survey of small volcanoes on the inner valley floor of the MAR (24°30'N), *Eos Trans. AGU*, *73* (14), 285, Spring Meeting suppl., 1992.

Solomon, S. C., P. Y. Huang, and L. Meinke, The seismic moment budget of slowly spreading ridges, *Nature*, *334*, 58–60, 1988.

Stein, R. S., G. C. P. King, and J. B. Rundle, The growth of geological structures by repeated earthquakes, 2, Field examples of continental dip-slip faults, *J. Geophys. Res.*, *93*, 13,319–13,331, 1988.

Stein, R. S., P. Briole, J.-C. Ruegg, P. Tapponnier, and F. Gasse, Contemporary, Holocene, and Quaternary deformation of the Asal Rift, Djibouti: Implications for the mechanisms of slow spreading ridges, *J. Geophys. Res.*, *96*, 21,789–21,806, 1991.

Toomey, D. R., S. C. Solomon, G. M. Purdy, and M. H. Murray, Microearthquakes beneath the median valley of the Mid-Atlantic Ridge near 23°N: Hypocenters and focal mechanisms, *J. Geophys. Res.*, *90*, 5443–5458, 1985.

Toomey, D. R., S. C. Solomon, and G. M. Purdy, Microearthquakes beneath median valley of Mid-Atlantic Ridge near 23°N: Tomography and tectonics, *J. Geophys. Res.*, *93*, 9093–9112, 1988.

Tucholke, B. E., Massive submarine rockslide in the rift-valley wall of the Mid-Atlantic Ridge, *Geology*, *20*, 129–132, 1992.

Vening Meinesz, F. A., Les Grabens Africans resultant de compression ou de tension dans la crôute terrestre?, *Inst. R. Colon. Belge Bull. Seances*, *21*, 539–552, 1950.

Weissel, J. K., and G. D. Karner, Flexural uplift of rift flanks due to mechanical unloading of the lithosphere during extension, *J. Geophys. Res.*, *94*, 13,919–13,950, 1989.

Whitmarsh, R. B., and A. S. Laughton, A long-range study of the Mid-Atlantic Ridge crest near 37°N (FAMOUS area) and its tectonic implications, *Deep Sea Res.*, *23*, 1005–1023, 1976.

Zuber, M. T., E. M. Parmentier, and R. C. Fletcher, Extension of continental lithosphere: A model for two scales of Basin and Range deformation, *J. Geophys. Res.*, *91*, 4826–4838, 1986.

J. Lin and P. R. Shaw, Woods Hole Oceanographic Institution, Woods Hole, MA 02543.